

## Interaction of Different Metal Ions with Carboxylic Acid Group: A Quantitative Study

Tanushree Bala,<sup>†</sup> B. L. V. Prasad,<sup>†</sup> Murali Sastry,<sup>\*,†,‡</sup> Mousumi Upadhyay Kahaly,<sup>§</sup> and Umesh V. Waghmare<sup>\*,§</sup>

Materials Chemistry Division, National Chemical Laboratory, Pune 411 008, India, and Theoretical Sciences Unit, Jawaharlal Nehru Centre for Advanced Scientific Research, Jakkur Post Office, Bangalore 560 064, India

Received: November 29, 2006; In Final Form: April 26, 2007

The binding strength of the carboxylic acid group (-COOH) with different divalent metal ions displays considerable variation in arachidic acid (AA) thin films. It is considered that in AA thin films the metal ions straddle the hydrophilic regions of the stacked bilayers of AA molecules via formation of carboxylates. In this study first the uptake of different divalent cations in films of AA is estimated by atomic absorption spectroscopy (AAS). Through the amount of cation uptake, it is found that the strength of binding of different cations varies as  $\text{Ca}^{2+} > \text{Co}^{2+} > \text{Pb}^{2+} > \text{Cd}^{2+}$ . Variation in the binding strength of different ions is also manifested in experiments where AA thin films are exposed to metal ion mixtures. The higher binding strength of AA with certain metal ions when exposed individually, as well as the preference over the other metal ions when exposed to mixtures, reveal some interesting deviation from the expected behavior based on considerations of ionic radii. For example,  $\text{Pb}^{2+}$  is always found to bind to AA much more strongly than  $\text{Cd}^{2+}$  even though the latter has smaller ionic radius, indicating that other factors also play an important role in governing the binding strength trends apart from the effects of ionic radii. Then, to get a more meaningful knowledge regarding the binding capability, first-principles calculations based on density functional theory have been applied to study the interaction of different cations with the simplest carboxylic acid, acetic acid, that can result in formation of metal diacetates. Their electronic and molecular structures, cohesive energies, and stiffness of the local potential energy well at the cation (M) site are determined and attempts are made to understand the diversity in geometry and the properties of binding of different metal ions with -COOH group. We find that the calculated M–O bond energies depend sensitively on the chemistry of M atom and follow the experimentally observed trends quite accurately. The trends in M–O bond energies and hence the total M–acetate binding energy trends can actually be related to their molecular structures that fall into different categories: Ca and Cd have tetrahedral coordination; Fe, Ni, and Co exhibit planar 4-fold coordination; and Pb is off-centered from the planar structure (forming pyramidal structure) due to its stereochemically active lone pair of electrons.

### Introduction

Complexation of different metal ions with a long-chain organic molecule having a functional head group can be of enormous importance for biological and technological applications. Metal ions can interact with various functional molecules starting from lipids,<sup>1</sup> polymers,<sup>2</sup> surfactants,<sup>3</sup> bolaamphiphiles,<sup>4</sup> or even with certain enzymes of bacteria<sup>5</sup> through ionic, covalent, or ion–dipole interactions, and each of them can be explicitly used for a range of applications. Among the different functional groups, the -COOH–metal ion interaction is probably the most important for several applications. For example, the interaction of polycarboxylates with metal ions is utilized in wastewater treatment for the selective removal of toxic metal ions<sup>6,7</sup> and also employed as high quality absorbing materials.<sup>8</sup> The adsorption behavior of metal ions on functionalized activated charcoal is also dependent on similar kind of interac-

tions and has great technological relevance,<sup>9</sup> particularly in the field of environmental science and catalysis.

Similarly, the -COOH group plays an important role in all biological systems as all proteins contain this group, and hence in recent years, there has been renewed interest in the study of metal ion–COOH interaction not only for its potential applications but also for the detailed understanding of the basic physics and chemistry involved in it. For example, binding of  $\text{Ca}^{2+}$  ions with the -COO<sup>-</sup> group of proteins can influence many biological processes like blood clotting, nerve cell transmission, etc.<sup>10,11</sup> The construction of an assembled layer of hybrid organic/inorganic composite materials that has received special attention is also dependent on the electrostatic interaction of the organic layer; and in many cases the -COOH head group/metal cation interaction plays a very significant role.<sup>12</sup> Carboxylic acid binding becomes imperative when nanoparticles are synthesized in a thermally evaporated fatty acid thin film by incorporating metal ions into the acid bilayer. Basically the stability of the nanoparticles thus formed is vastly contributed from the interaction of the two.<sup>13</sup> In fact, thin films can also be exploited for the synthesis of bimetallic alloys and the strength of metal–carboxylic acid bond will play the crucial role in tailoring the amount of incorporated metal cations in the film, which in turn

\* Authors to whom correspondence should be addressed: (U.V.W.) phone +91 80 22082842; fax +91 20 22082767; e-mail waghmare@jncasr.ac.in; (M.S.) phone 91 20 66218487; fax 91 20 66218490; e-mail msasr@tatachemicals.com.

<sup>†</sup> National Chemical Laboratory.

<sup>‡</sup> Present address: Tata Chemicals Ltd, Leela Business Park, Andheri (E), Mumbai – 400 059, India.

<sup>§</sup> Jawaharlal Nehru Centre for Advanced Scientific Research.

is the key to determine the composition of the alloy formed. It has already been witnessed that the insertion chemistry of cations into thin film is much more complex than that is understood from simple electrostatic interaction between the two depending on their charge to size ratio measured in terms of ionic radii.<sup>14</sup> Ordered supramolecular architectures that are generally achieved at air/water interface through the combination of metal ions with polymer or polycarboxylate monolayer is the result of the metal ion–carboxylic acid interaction.<sup>15</sup> In this case also, if the subphase contains a 1:1 mixture of various cations, the amount of different cations binding to the carboxylate monolayer never retains the same composition. For example, earlier work from Ganguly et al.<sup>16</sup> regarding the competitive binding of different cations like Pb and Cd with AA monolayer, using Langmuir–Blodgett techniques, clearly showed that Pb has higher binding strength than Cd though the size of  $\text{Pb}^{2+}$  is bigger than  $\text{Cd}^{2+}$ . At that time, the result was, qualitatively, allied with the complex equilibrium in the immersed phase between the  $\text{Pb}^{2+}$ ,  $\text{Cd}^{2+}$ , and  $\text{H}^+$  ions in the interlamellar regions and the solution phase,<sup>16</sup> though the exact reasons for such deviations were referred for further studies. It is also well-known in the field of nanotechnology that a variety of nanoparticles, for example, Co,<sup>17a,b</sup> Ni,<sup>17c</sup> Ag,<sup>18</sup> etc., can be capped and hence be stabilized by the -COOH moiety of long-chain organic acid. Thus it is pertinent that we understand this interaction thoroughly and if possible obtain a quantitative perspective explaining various factors affecting it so as to exploit its usage in various applications. Since the simple ionic radius-based explanations fail to describe the -COOH group–metal ion binding strength trends, more systematic investigations involving molecular modeling and charge density plots may enlighten us on the factors governing these interactions.

Therefore, in this paper we first obtain a quantitative perspective on the subject of binding of different cations with -COOH group by estimating the uptake of different individual divalent metal ions into AA thin films. Results obtained from mixtures of metal ion threw light on the competitive binding of different metal ions with AA and substantiated the trends obtained from individual ions. The trends are then analyzed by modeling the structures of different divalent metal ions with two acetate groups by use of first-principles density functional theory, resulting in quantitative figures regarding the binding ability of different metal ions. These results support the experimental observations and we find that the geometry plays a crucial role in determining of the strengths of binding of different cations with the carboxylic acid group.

## Experimental Details

Arachidic acid (eicosanoic acid,  $\text{C}_{20}\text{H}_{40}\text{O}_2$ , 99%), cobalt chloride hexahydrate ( $\text{CoCl}_2 \cdot 6\text{H}_2\text{O}$ , 99%), cadmium nitrate monohydrate [ $\text{Cd}(\text{NO}_3)_2 \cdot \text{H}_2\text{O}$ , 99%], lead nitrate [ $\text{Pb}(\text{NO}_3)_2$ ,  $\geq 99\%$ ], calcium chloride anhydrous ( $\text{CaCl}_2$ , 98%), and chloroform (99.0–99.4%) were purchased from Sigma and used as received.

In a typical experiment, thin films of arachidic acid (AA, molecular weight 312.5) of 200 Å thickness were thermally vacuum deposited, in an Edwards E306 vacuum coating unit operated at a pressure of  $1 \times 10^{-7}$  Torr, onto gold-coated AT-cut quartz crystals (for monitoring film thickness) and glass and Si(111) substrates for the metal ion binding experiments and their subsequent characterizations like atomic absorption spectroscopy (AAS), Fourier transform infrared (FTIR) spectroscopy, and energy-dispersive analysis of X-ray (EDAX). The lipid (AA) was deposited in vacuum by a process of sublimation at a

temperature not exceeding 80 °C for a period of 1 min. FTIR analysis of the thermally evaporated arachidic acid film, carried out on a Perkin-Elmer Spectrum One FTIR spectrometer operated at a resolution of  $4 \text{ cm}^{-1}$  in the diffuse transmittance mode, showed no evidence of thermal degradation of the lipid molecules. The film thickness was monitored by use of a quartz crystal microbalance (QCM) fitted to the deposition chamber. Energy dispersive analysis of X-ray (EDAX) measurements of the AA films and other samples on Si (111) substrates were carried out on a Leica Stereoscan-440 instrument equipped with a Phoenix EDAX attachment. Atomic absorption spectroscopy (AAS) was performed on an AAS 201 Chemito instrument.

Various ions were selected for the experimental purposes:  $\text{Cd}^{2+}$ ,  $\text{Pb}^{2+}$ ,  $\text{Ca}^{2+}$ , and  $\text{Co}^{2+}$ . The choice has been made in such a way that all of them are divalent but possess different ionic sizes. Five pairs were considered from the combination of two of the chosen cations, namely, (a)  $\text{Cd}^{2+}/\text{Pb}^{2+}$ , (b)  $\text{Cd}^{2+}/\text{Ca}^{2+}$ , (c)  $\text{Cd}^{2+}/\text{Co}^{2+}$ , (d)  $\text{Co}^{2+}/\text{Pb}^{2+}$ , and (e)  $\text{Co}^{2+}/\text{Ca}^{2+}$ . The experiments were performed in two different ways. (A) Experiment 1: The AA film was dipped in a solution where both the cations of the selected pair were present in 1:1 proportion. (B) Experiment 2: The AA film was immersed in the metal ion solutions of a particular pair one after the other.

The Si(111) and glass substrates with the thin films of AA of 200 Å thickness were immersed in aqueous 50 mL solution of 1:1 mixture of both the metal ions of a particular pair (experiment 1). The concentration was maintained at  $1 \times 10^{-2}$  M with respect to either of the ions with the pH of the solution above 5.5 to ensure the presence of the carboxylate anionic form of AA, as the  $\text{pK}_a$  of AA is  $\sim 4.82$ . The resulting dicarboxylate salts of different metal ions with arachidic acid films on Si-(111) and glass substrates were washed with double-distilled water to ensure the presence of occluded cations only, dried under flowing nitrogen, and then subjected to FTIR and EDAX investigation. At this stage, after analysis of the samples by FTIR and EDAX, the glass substrates were kept in 10 mL of double-distilled water with its pH adjusted to  $\sim 1.8$ – $2$  by dropwise addition of HCl. At this low pH the carboxylic acid groups are ensured to be reprotonated leaching out the metal ions entrapped inside the film of AA into water. Aliquots (10 mL) of these solutions were subjected to AAS measurements to estimate the amount of both the ions, which were dribbled out of AA films by simply changing the pH of the solution. The ratio of the concentration of the two ions from a particular pair can be related to the ratio of their bond strength. In principle, the concentration of the cations possessing higher binding strength should be found in excess in AA film; thus when these entrapped cations are leached out and examined by AAS technique, the solution is expected to contain that particular cation in larger quantity.

The cations bind to the carboxylate monolayer in a selective manner when a mixture of metal ions is present in the subphase and the film of metal–carboxylate can be lifted on substrates by the Langmuir–Blodgett technique at a particular surface pressure at which the monolayer is in its solid state (that ensures the most compact arrangement). When a few monolayers of the film are lifted on a substrate, it basically generates the same bilayer structure of AA with incorporated metal ions as we observe in the previous case. Thus, this experiment on LB verifies the result of the previous one. Surface pressure ( $\pi$ )–area (A) isotherms were measured in a Model 611 Nima LB trough at 25 °C with the compression and expansion speed for monolayer 100  $\text{cm}^2/\text{min}$ . AA (1 mg/mL) in chloroform was spread over a 1:1 solution mixture (concentration  $5 \times 10^{-3}$  M)

of the selected ion pair (subphase pH  $\sim$  5.5). Compression is allowed to start 10 min after spreading of the arachidic acid, to allow complete evaporation of chloroform. Thirty monolayers were deposited on a Si(111) substrate and the film was subjected to X-ray photoelectron spectroscopy (XPS) carried out on a VG MicroTech ESCA 3000 instrument at a pressure of  $1 \times 10^{-9}$  Torr. The general scan showing C 1s, O 1s, Cd 3d, and Pb 4f (for the first pair of cations) core level spectra were recorded with unmonochromatized Mg K $\alpha$  radiation (photon energy = 1253.6 eV) at a pass energy of 50 eV and electron takeoff angle (angle between electron emission direction and surface plane) of 60°. The overall resolution was  $\sim$ 1 eV for the XPS measurements. The core level spectra were background-corrected using the Shirley algorithm.<sup>19</sup> The core level binding energies (BE) were aligned with the adventitious carbon binding energy of 285 eV.

The preferential binding of a particular cation was rechecked by designing the second set of experiments (experiment 2). Si(111) and glass substrates, after deposition of AA layers, were immersed for 6–7 h in 50 mL of  $10^{-2}$  M aqueous solution of the metal ion having lower binding strength to the carboxylic acid group. In every case, the pH of the solutions was maintained above 5.5 to ensure complete deprotonation of AA. The resulting salts of different metal ions with arachidic acid films on Si(111) and glass substrates were washed thoroughly, dried with N<sub>2</sub> jet, and subjected to FTIR and EDAX investigation. Then the same substrates were dipped in the second metal ion solution having a higher complexation tendency with the carboxylic head group. The substrate were immersed for 6–7 h in the solutions and then treated in the same way as in the first step of the experiments. At this stage, after analysis of the samples by FTIR and EDAX, the Si and glass substrates were again treated with 10 mL of aqueous HCl with pH adjusted to  $\sim$ 2. This 10 mL solution was examined by AAS to determine the concentration of both the ions present there.

### Computational Details

Our calculations are based on first-principles density functional theory (DFT) with a generalized gradient approximation (GGA) to the many-electron exchange correlation energy as given by Perdew–Burke–Ernzerhof (PBE) functional.<sup>20</sup> We use PWSCF 2.0.1<sup>21</sup> implementation of DFT,<sup>22,23</sup> which employs plane-wave basis and ultrasoft pseudopotentials<sup>24</sup> to represent interaction between ions and electrons. Energy cutoff of 25 Ry is used on the plane-wave basis used in the representation of wavefunctions and that of 150 Ry for the representation of density. Periodic boundary conditions are used with a large supercell such that periodic images of molecules are separated by a vacuum of at least 12 Å along its axis and at least 8 Å perpendicular to its axis. This ensures negligible interaction between the periodic images of metal diacetate molecules. Resulting Brillouin zone is small and we use a single  $k$ -point (0, 0, 0) in its sampling.

Molecular structures are determined through total energy minimization with the Broyden–Fletcher–Goldfarb–Shanno (BFGS)<sup>25</sup> algorithm and Hellmann–Feynman forces on atoms. Structural optimization is carried out until the forces on all the atoms are less than 0.001 Ry/bohr. For acetic acid, calculated bond lengths (shown in Table 1) agree within 2% with their experimental values. These errors are typical of the density functional theory calculations with GGA. Calculated bond length of H<sub>2</sub> molecule is 0.75 Å, which also compares well with the experimental bond length of 0.74 Å. In determination of structures of metal diacetates, we used different initial struc-

**TABLE 1: Comparison of Different Bond Lengths in Acetic Acid**

	bond length $l_B$ , Å				
	C–H	C–C	C=O	C–O	O–H
our results	1.10	1.51	1.22	1.38	0.98
experiment	1.07	1.50	1.23	1.36	0.97

tures: planar (a) cis, (b) trans structure of metal diacetate, (c) metal diacetate with one acetate group aligned in a plane perpendicular to the other. All the initial structures were generated from experimental bond lengths.<sup>25</sup>

Cohesive energy of each metal diacetate molecule ( $E_c^M$ ) was estimated by subtracting total energies of its constituent atoms from the total energy of the molecule with optimized geometry. Energy as a measure of strength of the metal–acetate bond,  $E_{M-A}$ , was calculated as

$$E_{M-A} = 0.5[E_c^M + E_c^H - 2(E_c^{AA})]$$

where  $E_c^H$  is the cohesive energy for H<sub>2</sub> molecule and  $E_c^{AA}$  is the cohesive energy for acetic acid.

### Results and Discussion

To follow the experimental binding strength of ions with AA, we examined the films by different analytical techniques such as FTIR, AAS, SEM-EDAX, and XPS analysis. FTIR can be used to apprehend the qualitative features of binding. The other investigations can provide a quantitative basis for the binding strengths that have been used for further theoretical analysis. The films have been prepared in the following way for the procedure marked as experiment 1. First, a substrate with  $\sim$ 200 Å thick AA film is dipped in a mixture of the selected ion pair at a 1:1 molar ratio and at pH 5.5. It is expected that at this pH the -COOH groups are deprotonated and the cation will bind with the head group of the molecule. Further, to estimate the amount of metal ion uptake from the mixture of metal ions into AA films, the following simple technique is adapted. The films obtained as mentioned above, by dipping into the mixture of metal ions, are washed thoroughly with deionized water to remove any surface-adsorbed metal ions. These films are then dipped in an aqueous solution of pH 1.8. At this low pH the AA is reprotonated and the cations are released into the solution. The changes occurring in the FTIR spectra of AA films at various stages for dipping into the selected ion pair of Cd<sup>2+</sup>/Ca<sup>2+</sup> are discussed below. In the films of AA-Cd<sup>2+</sup> and AA-Ca<sup>2+</sup>, the carbonyl stretching frequency of pure AA (Figure 1, curve 1)<sup>26</sup> at 1693 cm<sup>-1</sup> is found to shift to 1531 cm<sup>-1</sup> (in the case of  $1 \times 10^{-2}$  M CdCl<sub>2</sub>; curve 2) and 1578 cm<sup>-1</sup> (in the case of  $1 \times 10^{-2}$  M CaCl<sub>2</sub>; curve 3). The shift to the lower wavenumber indicates a complexation between the head group and the cation present in the solution. The higher wavenumber vibration for Ca<sup>2+</sup> as compared to Cd<sup>2+</sup> clearly indicates that Ca<sup>2+</sup> is more strongly bound to the -COOH head group of AA than Cd<sup>2+</sup>. It is worth noting here that when an AA film first dipped in Cd<sup>2+</sup> ions is subsequently dipped in  $1 \times 10^{-2}$  M CaCl<sub>2</sub> solution, the carbonyl stretch vibration moves to  $\sim$ 1578 cm<sup>-1</sup> (curve 4) from the initial 1531 cm<sup>-1</sup> observed with Cd<sup>2+</sup> ions, indicating a replacement of Cd<sup>2+</sup> by Ca<sup>2+</sup> ions. Curve 5 in Figure 1 shows the FTIR spectrum after the films are dipped in aqueous solutions of pH 1.8. The carbonyl stretch reappears at its original frequency of 1693 cm<sup>-1</sup> (curve 5) after this acid treatment. The regeneration of -COOH stretch authenticates that this is an easy protocol to ooze out the entrapped

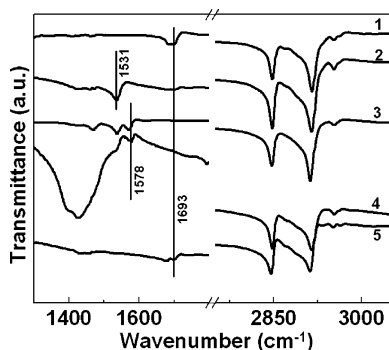


**Figure 1.** (Curve 1) FTIR spectrum of pure AA. (Curve 2) Spectrum after the substrate-containing AA film was dipped into  $\text{CdCl}_2$  solution for 4 h. (Curve 3) FTIR graph when AA film is treated with only  $\text{CaCl}_2$  solution. (Curve 4) Spectrum after AA- $\text{Cd}^{2+}$  film was plunged into the  $\text{CaCl}_2$  solution; the carbonyl peak shows a shift, indicating the replacement of  $\text{Cd}^{2+}$  by  $\text{Ca}^{2+}$ . (Curve 5) Spectrum of AA film with the cations after treatment with an aqueous solution of pH 1.8; the FTIR curve shows the feature of pure AA.

**TABLE 2: AAS Results Illustrating the Concentration Ratio of the Selected Ion Pairs in Arachidic Acid Films<sup>a</sup>**

selected ion pairs	AAS analysis	
	ion mixture taken in 1:1 molar ratio	ions taken one by one
Cd Pb	1:140	1:825
Cd Ca	1:10.7	1:10
Cd Co	1:6.29	1:13.4
Co Pb	1:2.67	1:3.78
Co Ca	1:0.67	1:0.79

<sup>a</sup> AA films are dipped into the 1:1 molar ratio mixture of the ions (column 2) or the films are dipped into the ionic solutions of the selected pair one after the other (column 3).

cations from the AA film very conveniently. The solutions obtained by the above mentioned acid treatment of the films prepared by the route experiment 1 are then subjected to AAS analysis.

The ratio of the concentration of different pair of ions as obtained from the AAS measurement is presented in Table 2. First, the trend between  $\text{Ca}^{2+}$  and  $\text{Cd}^{2+}$  for the experiment 1 case (Table 2, column 2) clearly agrees with the qualitative features observed in the FTIR analysis. Analysis of the full data shows that  $\text{Pb}^{2+}$  is dominantly bound to AA films as compared to  $\text{Cd}^{2+}$  and to some extent  $\text{Co}^{2+}$  too (especially when a  $\text{Pb}^{2+}$  exchange is done for  $\text{Co}^{2+}$ ).  $\text{Cd}^{2+}$  shows the lowest binding strength as compared to all the other cations ( $\text{Pb}^{2+}$ ,  $\text{Co}^{2+}$ , and  $\text{Ca}^{2+}$ ) involved in the set of experiments. The binding strengths of  $\text{Co}^{2+}$  and  $\text{Ca}^{2+}$  can be regarded as equivalent.

Taking hints from the above analysis, the second set of experiments (experiment 2) are performed wherein the AA films are dipped in different metal ion solutions sequentially. In the following we discuss results from two such pairs in more detail. For example, AAS analysis (Table 2, column 3) reveals that, for the  $\text{Cd}^{2+}/\text{Ca}^{2+}$  pair,  $\text{Ca}^{2+}$  must depict a stronger binding than the other cation. So in principle, when a AA- $\text{Cd}^{2+}$  composite film is exposed to  $\text{Ca}^{2+}$  ions, they should replace  $\text{Cd}^{2+}$  from the composite, and thus in AAS analysis we should see an excess of  $\text{Ca}^{2+}$  ions compared to  $\text{Cd}^{2+}$  ions. Similarly, for the  $\text{Cd}^{2+}/\text{Pb}^{2+}$  pair,  $\text{Pb}^{2+}$  is found to be bound almost 800 times more strongly than  $\text{Cd}^{2+}$  when the AA film is allowed to interact with the respective cations one by one. EDAX analysis on the film at the first step, when AA film is dipped only in  $\text{CdCl}_2$  solution, demonstrated 1.76 at. % Cd, indicating that for every 2.01 -COOH group there is one  $\text{Cd}^{2+}$ . When the same

**TABLE 3: Metal Diacetate Cohesive Energies and Respective M–A Bond Energies<sup>a</sup>**

metal diacetate $[\text{M}(\text{CH}_3\text{COO})_2]$	$E_{\text{ch}}^{\text{M}}$ (kJ/mol)	$E_{\text{M-A}}$ (kJ/mol)
$\text{Ca}(\text{CH}_3\text{COO})_2$	8449.145	249.063
$\text{Ni}(\text{CH}_3\text{COO})_2$	8376.872	212.926
$\text{Pb}(\text{CH}_3\text{COO})_2$	8287.706	168.343
$\text{Co}(\text{CH}_3\text{COO})_2$	8311.319	180.150
$\text{Fe}(\text{CH}_3\text{COO})_2$	8261.010	154.995
$\text{Cd}(\text{CH}_3\text{COO})_2$	7984.286	16.633

<sup>a</sup> For six types of metal diacetates, where  $\text{M} = \text{Ca}, \text{Pb}, \text{Ni}, \text{Cd}, \text{Fe},$  or  $\text{Co}$ .

film is investigated after treatment with  $\text{Pb}(\text{NO}_3)_2$ , the atomic percent Cd is found to be below the detection limit of EDAX and a concomitant increase in atomic percent  $\text{Pb}^{2+}$  is found; here also for every  $\text{Pb}^{2+}$  there are 2.04 -COOH groups. (The results are not shown here.) Thus it is clear that  $\text{Cd}^{2+}$  ions are almost fully replaced by  $\text{Pb}^{2+}$ , probably because of the stronger bond formation with the carboxylic acid group. Even in the case when both cations were taken in 1:1 concoction, the  $\text{Pb}^{2+}$  ions are showing extremely specific binding with the AA (Table 2, column 2). The specificity is also checked by spreading an AA monolayer on an equimolar mixture of the two ions ( $\text{Cd}^{2+}$  and  $\text{Pb}^{2+}$ ) at the air/water interface. When investigated by XPS, the film shows a prominent Pb 4f core level signal (inset B of Figure S-1 in Supporting Information), which can be fit with binding energies of 138.9 eV ( $4f_{7/2}$ ) and 144.0 eV ( $4f_{5/2}$ ) matching well<sup>27</sup> with the values reported for  $\text{Pb}^{2+}$ . The peaks observed for Cd 3d core level are very weak and no fitting could be performed, indicating that very small amounts of  $\text{Cd}^{2+}$  are present in the film (inset A of Figure S-1 in Supporting Information). The stability of the AA monolayer on ion mixtures is represented by the pressure–area isotherm and is presented in Supporting Information (Figure S-1). Thus the XPS spectra of  $\text{Cd}^{2+}$  and  $\text{Pb}^{2+}$  corroborate the binding strength trends discussed so far. In fact, all these results are found to follow the same trend as envisaged from the first set of experiments. The small discrepancy in the results of different modes of experiment can be considered to be within the experimental error. However, all these experimental results are in contradiction to expectation based on simple assumptions that the metal ions with larger ionic radii will have weaker binding strength; on the basis of this assumption,  $\text{Pb}^{2+}$  ions should have weaker binding energy than  $\text{Cd}^{2+}$  ions with -COOH groups. Hence our experimental results as well as earlier studies<sup>16</sup> clearly indicate the complexity of this interaction and the necessity to study them in more detail.

The quantitative modeling approach based on DFT studies shows that  $E_{\text{M-A}}$  for most of the acetates is between 150 and 250 kJ/mol, with a notable exception of the Cd–acetate bond, which has an energy 10 times smaller than the rest (Table 3). Each energy is also smaller than that of a covalent C–C bond or standard ionic bonds. This is possibly because the M–acetate bonding is of mixed ionic and covalent type. Second, negatively charged acetate groups on the two sides of M ion would repel each other, destabilizing the M–O bond partially and resulting in smaller energies  $E_{\text{M-A}}$ . The binding strength (Table 3) of the cations follows the following order:  $\text{Ca}^{2+} > \text{Ni}^{2+} > \text{Co}^{2+} > \text{Pb}^{2+} > \text{Fe}^{2+} > \text{Cd}^{2+}$ . The order is in good agreement with experimental observations. The only inconsistency is observed in case of the fifth selected pair, that is,  $\text{Co}^{2+}/\text{Pb}^{2+}$ . In this case  $\text{Co}^{2+}$  showed weaker binding than  $\text{Pb}^{2+}$ , but if their strength of binding with -COOH group from the calculated figures is considered, the result can be considered to be within experimental slip-up, though we have tried to address this issue in the latter part of the paper. The ratio of bond strength of  $\text{Co}^{2+}$  and  $\text{Ca}^{2+}$  predicts the presence of both cations in almost equal

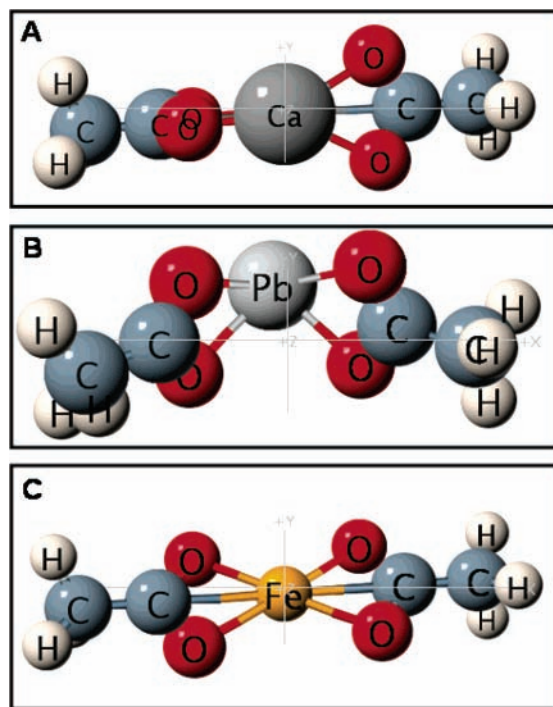


**Figure 2.** Representative relaxed energy minimum model of different metal diacetates: (A) tetragonal structures of calcium diacetate, (B) square pyramidal orientation of lead diacetate, and (C) square planar geometry of iron diacetate.

amounts in the solution prepared for AAS. In reality the AAS results followed the trend very closely (Table 2).

In fact, among the six different metal diacetates studied here, the structures are found to fall into three groups: (1) tetrahedral-like geometry, for  $M = \text{Ca}$  and  $\text{Cd}$ ; (2) square planar geometry, for  $M = \text{Ni}$ ,  $\text{Co}$ , and  $\text{Fe}$ ; and (3) square pyramidal geometry, for  $M = \text{Pb}$ . In Figure 2 we have demonstrated the relaxed minimum energy structures of three different metal diacetates, where  $M = \text{Ca}$ ,  $\text{Pb}$ , and  $\text{Fe}$  (panels A–C, respectively); that is, one from each structural group. The reasons for this grouping are the following:  $\text{Ca}^{2+}$  ion in calcium diacetate has outermost electronic structure as  $[\text{Ar}] 3d^0$ , whereas  $\text{Cd}^{2+}$  in cadmium diacetate has  $[\text{Kr}] 4d^{10}$ . For these two metal ions with completely empty or completely filled  $d$  orbitals, very weak crystal field splitting is expected and the electrostatic interactions arising from their strongly ionic nature result in tetrahedral-like structure (Figure 2A). The conclusion of their ionicity is based on partial density of electronic states analysis, which revealed that the lowest unoccupied molecular orbital (LUMO) exhibits a strong component of outermost  $s$ -electronic state of  $\text{Ca}$  and  $\text{Cd}$ , and the highest occupied molecular orbital (HOMO) is made of  $2p$  states of oxygen. Calculated HOMO–LUMO energy gaps in calcium and cadmium diacetates are 4.95 and 4.15 eV, respectively, indicating stronger ionic nature of the  $\text{Ca}$ –acetate bond.

Though lead diacetate has ionic  $\text{Pb}^{2+}$  (electronic configuration of  $\text{Pb}^{2+}$  is  $[\text{Xe}] 4f^{14} 5d^{10} 6s^2 6p^0$ ), it exhibits a rather different structure. Partial density of states of lead diacetate bears two important facts: (a) the LUMO has primarily the character of  $6p$  states of  $\text{Pb}$  and (b) while the HOMO is predominantly oxygen  $p$ -like, the state immediately below the HOMO has a strong character of the  $6s$  state of  $\text{Pb}$ . Also observed is contribution of the  $6s$  orbital of  $\text{Pb}$  to states about 4 eV lower in energy than the HOMO. The lone pair of electrons ( $6s$  state) of  $\text{Pb}$  is known to be stereochemically active, which results in off-centering of the  $\text{Pb}$  atom and lower symmetric structure of

oxides and chalcogenides.<sup>28</sup> We find it has the same effect here, leading to a square pyramidal structure (Figure 2B), where four oxygens remain in a plane and  $\text{Pb}$  is off-centered in the perpendicular direction along the line passing through the center. Our estimate of the HOMO–LUMO gap of lead diacetate is 4.46 eV.

$\text{Ni}^{2+}$ ,  $\text{Co}^{2+}$ , and  $\text{Fe}^{2+}$  ( $3d$  transition metals) in their respective diacetate forms have outermost valence electronic configurations  $[\text{Ar}] 3d^8$ ,  $[\text{Ar}] 3d^7$ , and  $[\text{Ar}] 3d^6$ , respectively; that is, they all have valence  $d$  orbitals more than half-filled (but  $<10$   $d$  electrons) and are expected to undergo strong crystal field splitting. For argument, we start from a tetrahedral coordination of the  $M$  ion in this case also, as in calcium and cadmium diacetates. In this case, a higher energy  $t_{2g}$  orbital is partially occupied (with four, three, and two electrons in the case of  $\text{Ni}$ ,  $\text{Co}$ , and  $\text{Fe}$ , respectively) and the system is unstable according to the Jahn–Teller theorem. Since these orbitals are planar, these transition metal diacetates seem to favor planar geometry (Figure 2C). Nickel diacetate is more symmetric with a completely filled doubly degenerate HOMO and has a zero magnetic moment, with a HOMO–LUMO gap of 1.29 eV. On the other hand, cobalt and iron diacetates possess geometries with further broken symmetry, resulting in closely spaced singly degenerate states near the HOMO and LUMO, with HOMO–LUMO gaps of 0.58 and 0.84 eV, respectively. Strong exchange and crystal field splitting result in magnetic moment of about  $3\mu_B$  and  $4\mu_B$  for cobalt and iron diacetates respectively. This is also reflected in the  $M$ – $\text{O}$  bond lengths: average bond length of  $\text{Ni}$ – $\text{O}$  is 1.91 Å, whereas those of  $\text{Co}$ – $\text{O}$  and  $\text{Fe}$ – $\text{O}$  bonds are 2.03 and 2.06 Å, respectively. We note that the average  $\text{Ca}$ – $\text{O}$ ,  $\text{Cd}$ – $\text{O}$ , and  $\text{Pb}$ – $\text{O}$  bond lengths are 2.29, 2.25, and 2.41 Å, respectively.  $\text{Pb}$ – $\text{O}$  bond length is expected to be larger due to stereochemical activity of its lone pair (which provides an additional coordination).

Since we relaxed structures starting from different initial structures, we now assess relative stability of different structures for a given metal diacetate, which gives a quantitative idea of different mechanisms leading to its stability. Energy of calcium diacetate in the tetrahedrally coordinated structure is 0.238 eV lower than its planar (cobalt diacetate-like) structure. Energy of the planar structure of cobalt diacetate is 1.261 eV lower than its tetrahedrally coordinated structure. Energy of lead diacetate in square pyramidal geometry is 1.099 eV lower than its energy in the tetrahedrally coordinated structure, whereas the energy of cadmium diacetate in the tetrahedral geometry is 1.062 eV lower than the energy of its square pyramidal structure. The trend in the calculated  $M$ – $\text{A}$  bond energies is rather similar to that in the energies of respective oxides (Figure 3) available in literature.<sup>25</sup> Calculated cohesive energies and consequent  $M$ – $\text{A}$  bond energies are found to be underestimated in comparison to the experimental data (obtained by summing up individual bond energies as approximated from [www.psi-gate.ac.uk](http://www.psi-gate.ac.uk)).

From Table 3, we see that lead diacetate is found to have  $M$ – $\text{O}$  bond energy almost 10 times that of cadmium diacetate. We try to understand this by examining the nature of bonding through electron densities and partial density of states. Lead diacetate is observed to have a special pyramidal structure (bouquet kind). Electronic charge density of lead diacetate (Figure 4A) reveals that there is a mixing of oxygen  $2p$  and  $\text{Pb}$   $6s$  orbitals in lead diacetate, indicating the partially covalent character of the  $\text{Pb}$ – $\text{O}$  bond [evident in Figure 4A (i)], whereas the asymmetric nature of the isosurface at a higher value of density indicates that the  $6s$  state of  $\text{Pb}$  is locally polarized

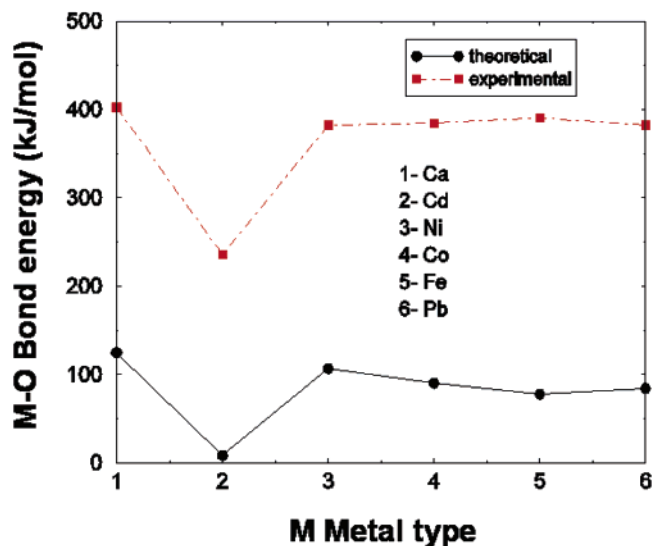


**Figure 3.** Comparison of calculated M–O bond energy with those from literature for different metal diacetates. Six points along  $x$ -axis denote six metal diacetates. Theoretical points (●, black) are obtained from our calculation (for metal diacetates), while experimental points (■, red) are from literature (M–O from metal oxide).

[Figure 4A (ii)], similar to its role in off-centering of Pb in ferroelectric materials.<sup>31</sup> On the other hand, isosurfaces of electron density of cadmium diacetate (Figure 4B) and calcium diacetate (Figure 4C) are consistent with ionic bonding between the metals and acetate groups. We observe an important feature particular to cadmium diacetate: there is an isosurface centered at the Cd site at a high value of density, which becomes more extended at lower densities. From the partial density of states, we find that (a) Cd is *not* completely ionic and (b) the fully occupied d states of Cd mix strongly with oxygen p states. The strength of this mixing estimated from the width of energy of d states is about 0.8 eV. This is similar to the p–d mixing in ZnO and GaN, where the energies of d and p states are comparable, resulting in their mixing.<sup>32</sup> Binding of Cd with acetates is weaker than that of Ca, due to its weaker ionic character, whereas binding of Pb is stronger than that of Cd due to an additional gain in energy from off-centering. Due to p–d coupling, we expect Cd displacements (along  $y$  and  $z$ ) to exhibit a shallow (less stiff) potential energy well and to couple well with strain.

In contrast to group II metals, the transition metals clearly show mixed ionic and covalent bonding with acetates. From the partial density of states, as mentioned earlier, Ni, Co, and Fe are in the 2+ ionic states. However, their d-states are at the HOMO and LUMO, giving rise to (a) covalent interactions with oxygens and (b) possibility of nonzero magnetic moment. As discussed earlier, nickel diacetate has a doubly degenerate HOMO that is fully occupied with a vanishing magnetic moment, whereas cobalt and iron diacetates have fewer d electrons and result in lower symmetry structure with magnetic moments of  $3\mu_B$  and  $4\mu_B$ , respectively. Thus, the shorter bond length of the Ni–O bond yields a stronger covalency while binding in nickel diacetate (Figure 4D; the O–C–O complex binds strongly with Ni). Cobalt diacetate (Figure 4E) exhibits relatively weaker M–O covalent bonds, resulting in decreasing strength of M–O bond as one goes from Ni to Fe along the row of the periodic table.

In order to understand the stiffness of binding of a metal ion M with acetate groups, we determined the self-force constant matrix (whose eigenvalues are proportional to the square of frequencies given in Table 4) of each M, which gives a harmonic

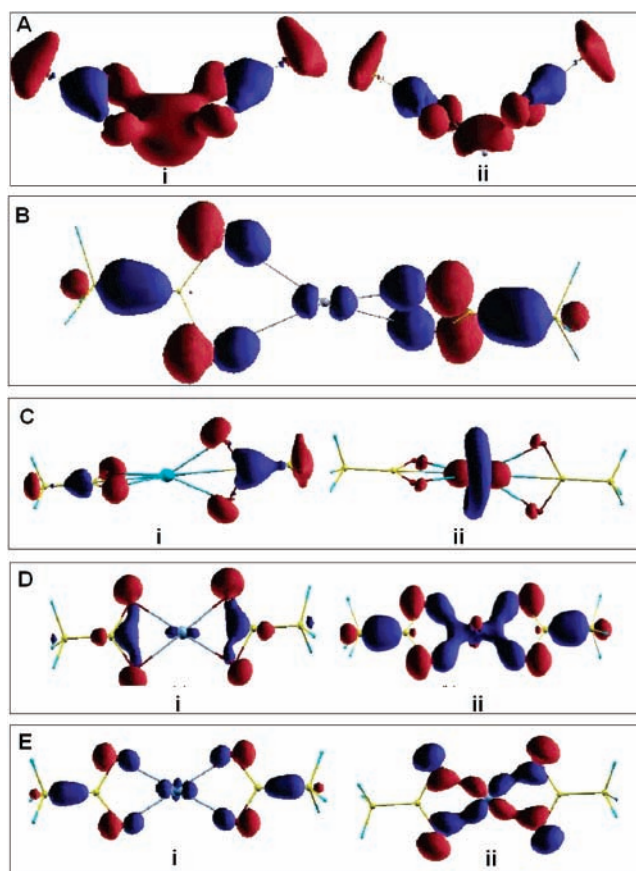


**Figure 4.** (A) Isosurface of charge densities of the Pb ion in lead diacetate: (i) at isovalue 0.002 e/bohr<sup>3</sup>, showing clear mixing of oxygen 2p and Pb 6s orbitals, and (ii) at isovalue 0.004 e/bohr<sup>3</sup>. (B) Isosurface of charge densities of cadmium diacetate with isovalue = 0.006 e/bohr<sup>3</sup>. (C) Isosurface of charge densities of the Ca ion in calcium diacetate: (i) at isovalue 0.007 e/bohr<sup>3</sup>, showing no mixing of oxygen 2p and Ca 4s orbitals, and (ii) at isovalue 0.003 e/bohr<sup>3</sup> for the first unoccupied band above the Fermi level. (D) Isosurface of charge densities of nickel diacetate: (i) at isovalue = 0.011 e/bohr<sup>3</sup>, showing no mixing of Ni 4s with O 2p states, and (ii) at isovalue = 0.006 e/bohr<sup>3</sup>, showing that Ni 3d states mix with O 2p states to produce partial covalent bonding. (E) Isosurface of charge densities of cobalt diacetate: (i) at isovalue = 0.011 e/bohr<sup>3</sup>, and (ii) at isovalue = 0.006 e/bohr<sup>3</sup>.

**TABLE 4: Self-Spring Constants and Local Vibrational Frequencies Associated with Motion of an M Ion in Metal Diacetate<sup>a</sup>**

M type	$\omega_1$ (cm <sup>-1</sup> )	$k_1$ (eV/Å <sup>2</sup> )	$\omega_2$ (cm <sup>-1</sup> )	$k_2$ (eV/Å <sup>2</sup> )	$\omega_3$ (cm <sup>-1</sup> )	$k_3$ (eV/Å <sup>2</sup> )
Ca	2203	18.154	978	3.570	942	3.270
Cd	1513	23.961	497	2.616	446	2.055
Pb	797	11.537	764	11.179	356	3.199
Ni	2626	37.720	2107	24.276	1099	6.607
Co	2141	25.233	1966	21.295	1482	11.891
Fe	1394	18.004	1360	12.021	696	2.676

<sup>a</sup> As determined from its self-force constant matrix.

description of the potential energy well faced by the motion of the M ion from its equilibrium position. We note that one can show, by use of the acoustic sum rule (or the translational invariance), that this stiffness is also a measure of the overall stiffness of bonding of the M ion with the rest of the molecule. Eigenvectors of the self-force constant matrix are the principal directions of stiffness of the local potential energy well of M. For calcium and cadmium diacetates, the potential energy well is stiffest ( $k_1$  in Table 4) along the axis of the molecule pointing toward carbon; it is relatively isotropic (expected from the

tetrahedral symmetry) and more than 2 times softer in the transverse plane ( $k_2$ ,  $k_3$ ). If one accounts for the difference in masses of Ca and Cd, it is clear that stiffness of the energy well for axial displacements of Cd is greater than that of Ca and that for displacements perpendicular to the axis is smaller, consistent with partial covalency of the Cd–acetate bond arising from p–d interactions. The energy well associated with motion of  $\text{Pb}^{2+}$  ion in its diacetate is relatively soft in comparison with Ca, and its anisotropy is quite different. Its stiffness along the axis of the molecule ( $797\text{ cm}^{-1}$ ) and along the off-centering (pyramidal axis) direction ( $764\text{ cm}^{-1}$ ) is comparable, while it is much softer along the direction perpendicular to these two. We note that the energy well of Cd displacements in the transverse plane is the softest of all. Structure of the transition metal (TM: Ni, Co, or Fe) diacetates is planar and the potential energy well is softest (shallowest) for displacements of a TM along the direction perpendicular to the molecular plane ( $k_3$ ). While the in-plane stiffness ( $k_1$ ,  $k_2$ ) of the potential energy well is higher and it decreases monotonically from Ni to Fe, there is an interesting feature: the principal axis corresponding to the highest stiffness is along the TM–C bond (molecular axis) in nickel and iron diacetates, whereas it is along the Co–O bond in cobalt diacetate. This correlates with the stiffest potential well of Co for out-of-plane displacements. In electronic structure too, cobalt diacetate is different from others in that its HOMO and LUMO have majority and minority spins, respectively. Overall, Ni–O bonds are the stiffest, which can be traced down to the shortest bond length of Ni–O. The trend in overall stiffness of TM–A bonds is very similar to that in their binding energies.

## Conclusion

In summary, this work shows that the binding strengths of different divalent metal ions with the carboxylic acid group shows interesting variations that cannot be explained by simple ionic radius considerations. For example,  $\text{Pb}^{2+}$  always exhibits stronger binding than  $\text{Cd}^{2+}$  though the ionic radius of the latter is smaller. Here we have obtained some quantitative estimates of the binding of divalent metal ions with carboxylic acids such as arachidic acid. The trends obtained from the experiments are then verified by the theoretical calculations. The binding of various inorganic metal ions with acetate groups is thoroughly analyzed through determination of the energy of binding and its quadratic curvatures with respect to motion of the metal ions. It is found that the geometries of these metal acetates fall in three categories: (a) tetrahedrally coordinated, strongly ionic Ca and Cd; (b) off-centered Pb ion, due to its lone pair of electrons; and (c) planar structures of the TM diacetates, with role of Jahn–Teller mechanisms. Cd is most weakly bound to acetates, and the energy associated with Cd displacements exhibits exceptional softness along the direction perpendicular to the molecular axis. We find that bonding of Cd with acetates is affected because of interaction between p states of oxygen with fully occupied d states of Cd, which are close in energy. Though the amount of cations interacting with the –COOH group of arachidic acid does not follow the exact values as obtained from the theoretical analysis, it can be rationalized as a difference between the ideal model preferred for calculations and the nonideality associated with the real systems. The strong bonding of  $\text{Pb}^{2+}$  with ligands as compared to  $\text{Cd}^{2+}$  at air–water interface could not be explained so far. In this paper, we have addressed this issue successfully, but the presence of  $\text{Pb}^{2+}$  ions about  $\sim 800$  times more than that of  $\text{Cd}^{2+}$  in AA film cannot be accounted at this moment with this model. It will be

addressed in the near future by considering other effects like hydration, orientation of the acid in solution, etc., that will offer more intimate details of a real system. Finally, our experimental results along with the theoretical explanations can probably be very helpful in many technological applications involving the metal ion–carboxylic acid interaction.

**Acknowledgment.** T.B. acknowledges the Council of Scientific and Industrial Research, Government of India, for a fellowship. T.B., B.L.V.P., and M.S. thank the DST for funding through DST-UNANST. M.U.K. and U.V.W. acknowledge use of the central computing facility of JNCASR and also a JNCASR conference on Chemistry of Materials, which initiated this collaboration.

**Supporting Information Available:** Pressure–area isotherm of pure AA spread over the subphase of an equimolar mixture of  $\text{Cd}^{2+}$  and  $\text{Pb}^{2+}$ , and XPS spectra of ions performed on a film lifted from the LB trough at a pressure of 30 mN/m. This information is available free of charge via the Internet at <http://pubs.acs.org>.

## References and Notes

- (1) (a) Shankar, S. S.; Rautaray, D.; Pasricha, R.; Pavaskar, N. R.; Mandale, A. B.; Sastry, M. *J. Mater. Chem.* **2003**, *13*, 1108 (b) Rautaray, D.; Sainkar, R.; Sastry, M. *Chem. Mater.* **2003**, *15*, 2809.
- (2) Moreno-Villoslada, I.; Rivas, B. L. *J. Phys. Chem. B* **2002**, *106*, 9708.
- (3) (a) Custers, J. P. A.; Kelemen, P.; Van den Broeke, L. J. P.; Stuart, M. A. C.; Keurentjes, J. T. F. *J. Am. Chem. Soc.* **2005**, *127*, 1594. (b) Shivshankar, S.; Patil, U.; Prasad, B. L. V.; Sastry, M. *Langmuir* **2004**, *20*, 8853.
- (4) (a) Lu, Q.; Luo, Y.; Li, L.; Liu, M. *Langmuir* **2003**, *19*, 285. (b) Buller, R.; Cohen, H.; Jensen, T. R.; Kjaer, K.; Lahav, M.; Leiserowitz, L. *J. Phys. Chem. B* **2001**, *105*, 11447.
- (5) Larrabee, J. A.; Leung, C. H.; Moore, R. L.; Thamrong-nawasawat, T.; Wessler, B. S. H. *J. Am. Chem. Soc.* **2004**, *126*, 12316.
- (6) Rivas, B. L.; Pereira, E. D.; Moreno-Villoslada, I. *Prog. Polym. Sci.* **2002**, *28*, 173.
- (7) (a) Boerlage, S. F. E.; Kennedy, M. D.; Bremere, I.; Witkamp, G. J.; Vander-Hoek, J. P.; Schippers, J. C. *J. Membr. Sci.* **2002**, *197*, 251. (b) Bonne, P. A. C.; Hofman, J. A. M. H.; vander Hoek, J. P. *Desalination* **2000**, *132*, 109.
- (8) Kazanskii, K. S.; Dubrovskii, S. A. *Adv. Polym. Sci.* **1992**, *104*, 97.
- (9) Xiao, B.; Thomas, K. M. *Langmuir* **2004**, *20*, 4566.
- (10) Iwasa, K.; Tasaki, I.; Gibbons, R. C. *Science* **1980**, *210*, 338.
- (11) Tasaki, I.; Byrne, P. M. *Biopolymers* **1994**, *34*, 209.
- (12) *Hybrid Organic–Inorganic Composites*; Mark, J. E., Lee, C. Y.-C., Bianconi, P. A., Eds.; ACS Symposium Series 585; American Chemical Society: Washington, DC, 1995.
- (13) Mandal, S.; Sastry, M. *Mater. Res. Bull.* **2002**, *37*, 1613.
- (14) *Nanoparticles Building Blocks for Nanotechnology*; Rotello, V., Ed.; Kluwer Academic/Plenum Publishers: New York, 2004; pp 225–250.
- (15) (a) Sastry, M.; Patil, V.; Mayya, K. S. *J. Phys. Chem. B* **1997**, *101*, 1167. (b) Mann, S. *Nature* **1988**, *332*, 119.
- (16) (a) Ganguly, P.; Paranjape, D. V.; Pal, S.; Sastry, M.; *Langmuir* **1994**, *10*, 1670. (b) Ganguly, P.; Pal, S.; Sastry, M.; Shashikala, M. N. *Langmuir* **1995**, *11*, 1078.
- (17) (a) Bala, T.; Arumugam, S.; Pasricha, R.; Prasad, B. L. V.; Sastry, M. *J. Mater. Chem.* **2004**, *14*, 1057. (b) Fu, L.; Liu, X.; Zhang, Y.; Dravid, V. P.; Mirkin, C. A. *Nano Lett.* **2003**, *3*, 757. (c) Bala, T.; Bhame, S. D.; Joy, P. A.; Prasad, B. L. V.; Sastry, M. *J. Mater. Chem.* **2004**, *14*, 2941.
- (18) (a) Bala, T.; Swami, A.; Prasad, B. L. V.; Sastry, M. *J. Colloid Interface Sci.* **2005**, *283*, 422. (b) Wang, W.; Efrima, S.; Regev, O.; *Langmuir* **1998**, *14*, 602. (c) Wang, W.; Chen, X.; Efrima, S. *J. Phys. Chem. B* **1999**, *103*, 7238.
- (19) Shirley, D. A. *Phys. Rev. B* **1972**, *5*, 4709.
- (20) Perdew, J. P.; Burke, K.; Ernzerhof, M. *Phys. Rev. Lett.* **1998**, *80*, 891.
- (21) Baroni, S.; Corso, A. D.; Gironcoli, S.; Giannozzi, P. <http://www.pwscf.org>.
- (22) Hohenberg, P.; Kohn, W. *Phys. Rev.* **1964**, *136*, 863B.

- (23) Kohn, W.; Sham, L. J. *Phys. Rev.* **1965**, *140*, 1133A.
- (24) Vanderbilt, D. *Phys. Rev. B* **1990**, *41*, 7892.
- (25) Lide, D. R., Ed. In *CRC Handbook of Chemistry and Physics*, 77th ed.; CRC Press: Boca Raton, FL, 1996.
- (26) <http://www.library.cornell.edu/nt/bookcpdf/c10-7.pdf>.
- (27) *The Aldrich Library of Infrared Spectra*, edition III; Pouchart, C. J., Ed.; Aldrich Chemical Co.: Milwaukee, WI, 1981; pp 283 and 286.
- (28) Wagner, C. D.; Riggs, W. M.; Davis, L. E.; Moulder, J. F. *Handbook of X-ray Photoelectron Spectroscopy*; Muilanberg, G. E., Ed.; Perkin-Elmer: Eden Prairie, MN, 1979; pp 160–161.
- (29) Waghmare, U. V.; Hill, N. A.; Kandpal, H.; Seshadri, R. *Phys. Rev. B* **2003**, *67*, 125111.
- (30) Waghmare, U. V.; Rabe, K. M. In *Materials Fundamentals of Gate Dielectrics*; ed. A. A. Demkov, A. A., and A. Navrotsky, A., Eds.; Springer: Dordrecht, The Netherlands, 2005; pp 215.